4 CdTe/CZT Spectrometers with 3-D Imaging Capabilities

Ezio Caroli and Stefano del Sordo

CONTENTS

4.1 INTRODUCTION

Semiconductor detector technology has dramatically changed the broad field of x-ray and γ-ray spectroscopy and imaging. Semiconductor detectors, originally developed for particle physics applications, are now widely used for x/γ-ray spectroscopy and imaging in a wide variety of fields, including, for example, x-ray fluorescence, γ-ray monitoring and localization, noninvasive inspection and analysis, astronomy, and diagnostic medicine. The success of semiconductor detectors is due to several unique characteristics, such as excellent energy resolution, high detection efficiency, and the possibility of development of compact and highly segmented detection systems. Among semiconductor devices, silicon (Si) detectors are the key detectors in the soft x-ray band (<15 keV). Si-PIN diode detectors [1] and silicon drift detectors (SDDs) [2], operated with moderate cooling by means of small Peltier cells, show excellent spectroscopic performance and good detection efficiency below 15 keV. On the other hand, germanium (Ge) detectors are unsurpassed for high-resolution spectroscopy in the hard x-ray energy band (>15 keV) and will continue to be the first choice for laboratory-based high-performance spectrometers [3].

However, in the last decades, there has been an increasing demand for the development of room-temperature detectors with compact structure having the portability and convenience of a scintillator but with a significant improvement in energy resolution and spatial resolution. To fulfil these requirements, numerous

high-Z and wide bandgap compound semiconductors have been exploited [4,5]. In fact, as demonstrated by the impressive increase in the scientific literature and technological development around the world, cadmium telluride (CdTe) and cadmium zinc telluride (CdZnTe or simply CZT)-based devices are today dominating the room-temperature semiconductor applications scenario, being widely used for the development of x/γ-ray instrumentation [6–8].

As already mentioned, for purely spectroscopic applications in the hard x-ray and γ-ray regime, germanium detectors have retained their supremacy, while applications that require imaging capabilities with high spatial resolution, possibly coupled with good spectroscopic performance (at room temperature), define the field in which the potential and advantages of CdTe/CZT-technology sensors can be fully exploited. In fact, the possibility of quite easily segmenting the charge-collecting electrodes in strips or arrays, as well as assembling a mosaic of even small sensitive units (i.e., crystals), makes it possible to obtain devices with intrinsically excellent bidimensional spatial resolution (down to tens of microns) and, according to the type of readout electronics, also to measure the energy released by the interaction of photons with the material (see [9,10] and other chapters in this book).

In this chapter, we will focus on a particular type of detector based on sensitive elements of CZT/CdTe, namely, spectrometers with spatial resolution in three dimensions. These, in fact, represent the new frontiers for applications in different fields that require increasing performance, such as high-energy astrophysics, environmental radiation monitoring, medical diagnostics with positron emission tomography (PET), and inspections for homeland security. The advantages offered by the possibility of reconstructing both the position of interaction of the incident photons in three dimensions (3-D) and the energy deposited by each interaction are of fundamental importance for applications that require high detection efficiency even at high energies (>100 keV), that is, in the Compton-scattering regime, as well as a wide-field localization of the direction of incidence and a uniform spectroscopic response throughout the sensitive volume. In fact, the possibility of reconstructing the photon interaction position in 3-D will allow correction for signal variations due to charge trapping and material nonuniformity, and will therefore allow the sensitive volume of each detector unit to be increased without degrading the spectroscopic performance.

4.2 X- AND γ-RAY SPECTROSCOPY WITH CZT/CdTe SENSORS

The typical operation of semiconductor detectors is based on collection of the charges created by photon interactions through the application of an external electric field. The choice of the proper semiconductor material for a radiation detector is mainly influenced by the energy range of interest. Among the various interaction mechanisms of x-rays and γ-rays with matter, three effects play an important role in radiation measurements: photoelectric absorption, Compton scattering, and pair production. In photoelectric absorption, the photon transfers all its energy to an atomic electron, while a photon interacting through the Compton process transfers only a fraction of its energy to an outer electron, producing a hot electron and a degraded photon; in pair production, a photon with energy above a threshold energy

of 1.02 MeV interacts within the Coulomb field of the nucleus, producing an electron and positron pair. Neglecting the escape of characteristic x-rays from the detector volume (the so-called fluorescent lines), only the photoelectric effect results in the total absorption of the incident energy and thus gives useful information about the photon energy. The interaction cross sections are highly dependent on the atomic number. In photoelectric absorption, it varies as $Z^{4,5}$, Z for Compton scattering, and Z^2 for pair production.

4.2.1 CdTe/CZT used as X- and γ-Ray Spectrometer

An optimum spectroscopic detector must favor photoelectric interactions, and so semiconductor materials with a high atomic number are preferred. Figure 4.1a shows the linear attenuation coefficients, calculated by using tabulated interaction cross-section values [11], for photoelectric absorption and Compton scattering of Si, CdTe, HgI_2, NaI, and BGO; NaI and BGO are solid scintillator materials typically used in radiation measurement. As shown in Figure 4.1a, photoelectric absorption is the main process up to about 200 keV for CdTe. The efficiency for CdTe detectors versus detector thickness and at various typical photon energies is reported in Figure 4.1b. A 10 mm thick CdTe detector ensures good photoelectric efficiency at 140 keV (>90%), while a 1 mm thick CdTe detector is characterized by a photoelectric efficiency of 100% at 40 keV.

Semiconductor detectors for x- and γ-ray spectroscopy behave as solid-state ionization chambers operated in pulse mode. The simplest configuration is a planar detector, which is a slab of a semiconductor material with metal electrodes on the opposite faces of the semiconductor (Figure 4.2). Photon interactions produce electron–hole pairs in the semiconductor volume through the discussed interactions. The interaction is a two-step process, whereby the electrons created in the photoelectric or Compton process lose their energy through electron–hole ionization. The most important feature of photoelectric absorption is that the number of electron–hole pairs is proportional to the photon energy. If E is the incident photon energy, the number of electron–hole pairs N is equal to E/w, where w is the average

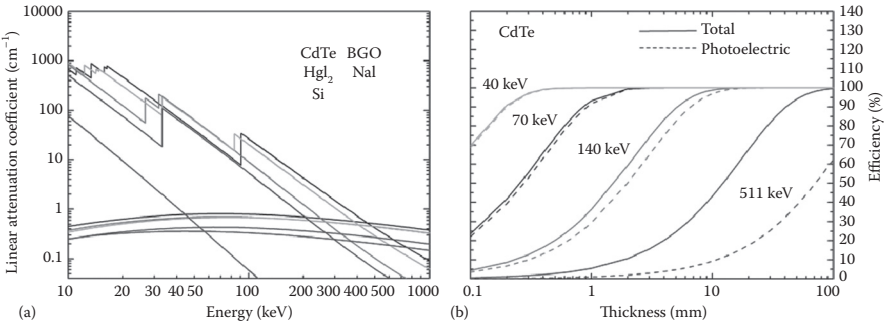

FIGURE 4.1 (See color insert) (a) Linear attenuation coefficients for photoelectric absorption and Compton scattering of CdTe, Si, HgI_2, NaI, and BGO. (b) Efficiency of CdTe detectors as a function of detector thickness at various photon energies.

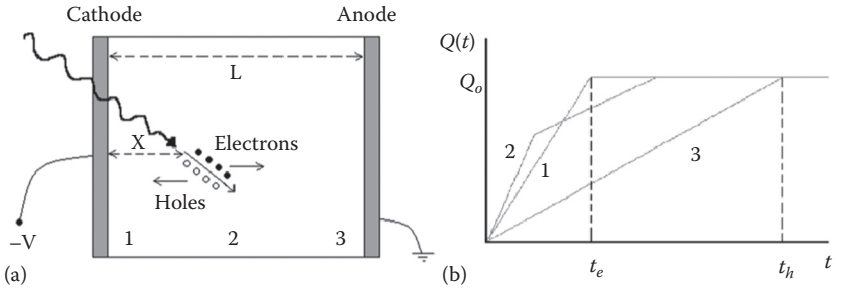

FIGURE 4.2 Planar configuration of a semiconductor detector: (a) Electron–hole pairs, generated by radiation, are swept toward the appropriate electrode by the electric field; (b) the time dependence of the induced charge for three different interaction sites in the detector (positions 1, 2, and 3). The fast-rising part is due to the electron component, while the slower component is due to the holes.

pair-creation energy. The generated charge cloud is $Q_0 = eE/w$. The electrons and holes move toward the opposite electrodes, anode and cathode for electrons and holes, respectively (Figure 4.2).

The movement of the electrons and holes causes variation ΔQ of induced charge on the electrodes. It is possible to calculate the induced charge ΔQ by the Shockley–Ramo theorem [12,13], which makes use of the concept of a weighting potential, defined as the potential that would exist in the detector with the collecting electrode held at unit potential, while all other electrodes are held at zero potential. According to the Shockley–Ramo theorem, the charge induced by a carrier q, moving from x_i to x_f, is given by Equation 4.1:

$$\Delta Q = -q\left[\varphi(x_f) - \varphi(x_i)\right] \tag{4.1}$$

where $\varphi(x)$ is the weighting potential at position x. It is possible to calculate the weighting potential by analytically solving the Laplace equation inside a detector [14]. In a semiconductor, the total induced charge is given by the sum of the induced charges due to both electrons and holes.

Charge trapping and recombination are typical effects in compound semiconductors and may prevent full charge collection. For a planar detector, having a uniform electric field, neglecting charge detrapping, the charge-collection efficiency (CCE), that is, the induced charge normalized to the generated charge, can be evaluated by the Hecht equation [15] and derived models [16] and is strongly dependent on the photon interaction position. This dependence, coupled with the random distribution of photon interaction points inside the sensitive volume, increases the fluctuations on the induced charge and produces peak broadening in the energy spectrum as well as the characteristic low tail asymmetry in the full energy peak shape observed in the planar CdTe/CZT sensor.

The charge transport properties of a semiconductor, expressed by the hole and electron mobility lifetime products ($\mu_h\tau_h$ and $\mu_e\tau_e$), are key parameters in the

development of radiation detectors. Poor mobility lifetime products result in short mean drift length λ and therefore small λ/*L* ratios, which limit the maximum thickness and energy range of the detectors. Compound semiconductors, generally, are characterized by poor charge transport properties due to charge trapping. Trapping centers are mainly caused by structural defects (e.g., vacancies), impurities, and irregularities (e.g., dislocations, inclusions). In compound (CdTe and CZT) semiconductors, the $\mu_e\tau_e$ is typically of the order of 10^{-5}–10^{-3} cm^2 V^{-1}, while $\mu_h\tau_h$ is usually much worse, with values around 10^{-6}–10^{-4} cm^2 V^{-1}. Therefore, the corresponding mean drift lengths of electrons and holes are 0.2–20 mm and 0.02–2 mm, respectively, for typical applied electric fields of 2000 V cm^{-1} [17].

The charge-collection efficiency is a crucial property of a radiation detector, affecting spectroscopic performance, and in particular energy resolution. High charge-collection efficiency ensures good energy resolution, which also depends on the statistics of the charge generation and the noise of the readout electronics. Therefore, the energy resolution (FWHM) of a radiation detector is mainly influenced by three contributing factors:

$$\Delta E = \sqrt{(2.355)^2 (F \cdot E \cdot w) + \Delta E_{\text{el}} + \Delta E_{\text{coll}}} \tag{4.2}$$

The first contribution is the Fano noise due to the statistics of the charge-carrier generation. In semiconductors, the Fano factor *F* is much smaller than unity (0.06–0.14) [18]. The second contribution is the electronic noise, which is generally measured directly using a precision pulser, while the third term takes into account the contribution of the charge-collection process. Different semiempirical relations have been proposed for the charge-collection contribution evaluation of different detectors [19].

Figure 4.3 shows a typical spectroscopic system based on a semiconductor detector. The detector signals are amplified by a charge-sensitive preamplifier (CSA) and then shaped by a linear amplifier (shaping amplifier). Energy spectra are obtained by a multichannel analyzer (MCA), which samples and records the shaped signals.

As pointed out in the foregoing discussions, poor hole-transport properties of CdTe and CdZnTe materials are a critical issue in the development of x- and γ-ray detectors. Hole trapping reduces the charge-collection efficiency of the detectors and produces asymmetry and a long tail in the photopeaks in the measured spectra (hole tailing). Several methods have been used in order to minimize this effect.

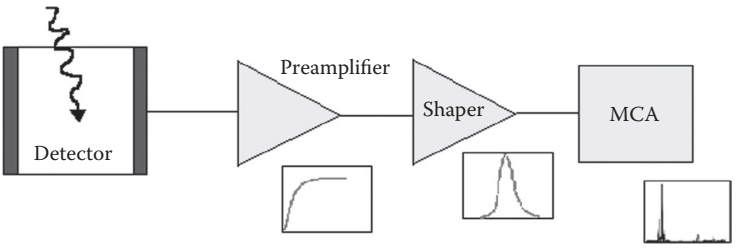

FIGURE 4.3 Block diagram of a standard spectroscopic detection system for x- and γ-rays.

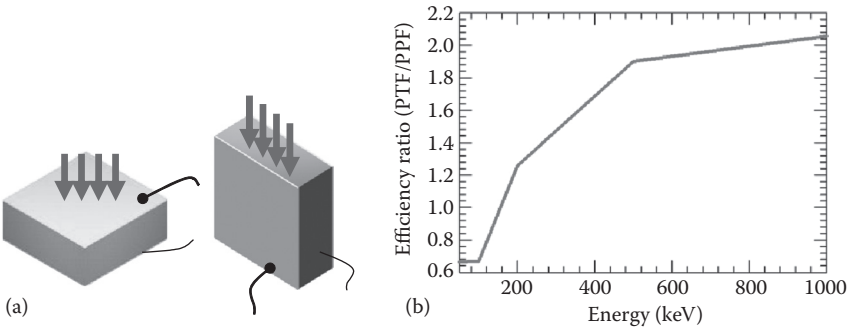

FIGURE 4.4 (a) Usual irradiation configuration in which photons impinge (arrows) the detector through the cathode surface (PPF: planar parallel field) and the PTF (planar transverse field) in which the photons impinge on the sensor orthogonally with respect to the charge collecting field. (b) Ratio between PTF and PPF efficiency calculated in [21] for impinging photon energies from 50 to 1000 keV, assuming PTF thickness equal to 10 mm and distance between electrodes (i.e., the PPF absorption thickness) 2.5 mm.

Some techniques concern the particular irradiation configuration of the detectors (see Figure 4.4a). Planar parallel field (PPF) is the classical configuration used in overall planar detectors, in which the detectors are irradiated through the cathode electrode, thus minimizing the hole-trapping probability. In an alternative configuration, denoted planar transverse field (PTF) [20], the irradiation direction is orthogonal (transverse) to the electric field. In such a configuration, different detector thicknesses can be chosen, in order to fit the detection efficiency required, without modifying the interelectrode distance and thus the charge-collection properties of the detectors. This technique is particularly useful to develop detectors with high detection efficiency in the γ-ray energy range. Figure 4.4b shows a plot of the ratio between the efficiency achievable by a CdTe spectrometer with lateral sides of 10 mm and a distance between electrodes of 2.5 mm [21]. This plot shows that the PTF irradiation configuration becomes favorable in terms of detection efficiency above 200 keV.

4.2.2 Spectroscopic Performance Improvement Techniques

Different methods have been proposed to compensate for the trapping effects in CdTe/CZT semiconductor detectors in order to improve their spectroscopic resolution toward its theoretical limit and to increase their full energy efficiency. The most frequently used methods rely on the possibility of avoiding the contribution of holes to the formation of the charge signal, thus using the CZT/CdTe detector as a single-charge sensing device. In this configuration, only electrons are collected. Because of their mobility characteristics, the effect of trapping is limited and can be further compensated for using information derivable from simple signal manipulation.

Several techniques are used in the development of detectors based on the collection of electrons (single-charge carrier sensitive), which have better transport properties

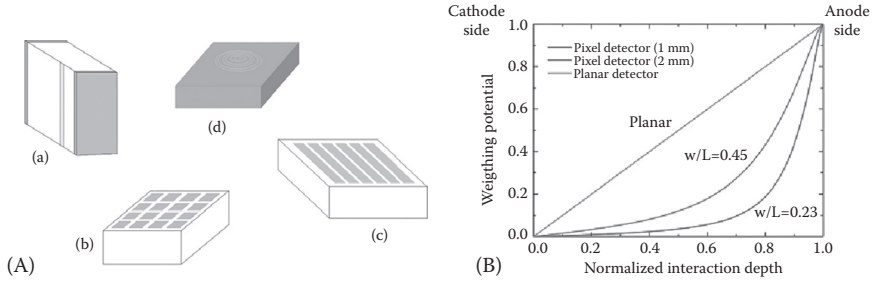

FIGURE 4.5 **(See color insert)** (A) Single-charge collection electrode configurations widely used in CdTe and CdZnTe detectors: (a) parallel-strip Frisch grid, (b) pixel, (c) strip, and (d) multiple electrodes. (B) Weighting potential of a pixel detector, compared with a planar detector. It is possible to improve the unipolar properties of pixel detectors by reducing the *w/L* ratio (i.e., pixel size to detector thickness), according to the theory of small pixel effect.

than holes. Single-charge carrier-sensing techniques are widely employed for CdTe and CdZnTe detectors (unipolar detectors), both by using electronic methods (pulse rise time discrimination [22], biparametric analysis [23,24]) and by developing careful electrode design (Frisch grid [25,26], pixels [27,28], coplanar grids [29], strips [30,31], multiple electrodes [32–34]). Figure 4.5 shows some unipolar electrode configurations widely used in CdTe and CdZnTe detectors.

The first single-charge carrier-sensing technique was implemented in gas detectors by Frisch [35] to overcome the problem of slow drift and loss of ions. A simple semiconductor Frisch grid detector and a derivate structure known as the coplanar-grid configuration can be built by using parallel metal strips on the opposite faces of the detector (yellow strips of Figure 4.5a) connected in an alternating manner to give two sets of interdigital grid electrodes. Pixels and strips on the anode electrode of detectors (Figure 4.5b, c), useful for their imaging properties, are also characterized by unipolar properties. The small-size anode electrode and the multiple ring electrodes (drift electrodes) on the anode surface of the detectors, as shown in Figure 4.5d, optimize charge collection, minimizing the effect of the hole trapping on the measured spectra.

In general, the almost unipolar characteristics of these detector configurations are due to the particular shape of the weighting potential: it is low near the cathode and rises rapidly close to the anode. According to this characteristic, the charge induced on the collecting electrode, proportional to the weighting potential, as stated by the Shockley–Ramo theorem, is mostly contributed by the drift of charge carriers close to the anode, that is, the electrons. On the contrary, the linear shape of the weighting potential of a planar detector makes the induced charge sensitive to both electrons and holes, as discussed above.

In particular, the introduction of coplanar-grid noncollecting electrodes in the anode-side design of the sensor provides an important additional feature that is fundamental to realizing 3-D sensing spectrometers, that is, the position information of the radiation interaction point inside the sensitive volume [29]. In fact, for these electrode configurations, the induced charge on the planar cathode Q_p increases

roughly as a linear function of the distance D of γ-ray interaction location from the coplanar anodes ($Q_p \propto D \times E_\gamma$), because it is proportional to the drift time of electrons. On the other hand, the coplanar anode signal Q_s is only approximately proportional to the γ-ray deposited energy ($Q_s \propto E_\gamma$). Therefore, the interaction depth can be estimated by reading both Q_p and Q_s signal amplitude for each interaction through their ratio (also called depth parameter): $d = Q_p/Q_s$, $\propto D$ [36].

4.3 3-D CZT/CdTe SENSOR CONFIGURATIONS

A 3-D spectrometer is, in principle, a detector divided into volume elements (voxels), each operating as an independent spectroscopic sensor. The signal produced in each voxel by the interaction of an incoming x/γ photon must be able to be read and converted into a voltage signal proportional to the energy released. If the readout electronics of the detection system implements a coincidence logic, it will be possible to determine to some extent the history of the incident photon inside the sensitive volume by associating the energy deposits in more voxels with the same incident photon.

The need for this type of sensor comes from application requirements. For example, in the field of hard x- and soft γ-ray astrophysics (10–1000 keV), there are promising developments of new focusing optics operating for up to several hundreds of kiloelectronvolts through the use of broadband Laue lenses [37] and a new generation of multilayer mirrors [38]. These systems make it possible to push the sensitivity of a new generation of innovative high-energy space telescopes to levels far higher (100–1000 times) than current instrumentation. To obtain the maximum return from this type of optics up to the megaelectronvolt level requires the use of focal plane detectors with high efficiency (>80%) even at higher energies, and with that the ability to measure the energy spectrum with good spectroscopic resolution and also to localize accurately (0.1–1 mm) the point of interaction of the photons used for the correct attribution of their direction of origin in the sky.

In fact, the realization of 3-D spectrometers by a mosaic of single CdTe/CZT crystals is not as easy as in the case of bidimensional imagers, mainly due to the small dimension of each sensitive unit, necessary to guarantee the required spatial resolution, and also the intrinsic difficulty of packaging in 3-D sensor units, in which each one requires an independent spectroscopic readout electronics chain. A solution is offered by the realization of a stack of 2-D spectroscopic imagers [39,40]. This configuration, while very appealing for large-area detectors, has several drawbacks for application, requiring fine spatial resolution in three dimensions and compactness. Indeed, the distance between 2-D layers of the stack limits the accuracy and the sampling of the third spatial coordinate, and passive materials are normally required for mechanical support.

To solve this kind of problem, in the last 10–15 years several groups have focused their activity on the development of sensors based on high-volume (1–10 cm^3) crystals of CZT/CdTe capable of intrinsically operating as 3-D spectrometers and therefore able to meet the requirements for certain applications, or to make more efficient and easy the realization of 3-D detectors based on matrices of these basic units. The main benefits are: a limited number of required readout channels to achieve

the same spatial resolution; packing optimization; and reduction of passive material between sensitive volumes. In these developments, a key role is played by the adopted electrode configuration. As already seen in Section 4.2.2, various electrode configurations have been proposed and studied to improve both the spectroscopic performance and the uniformity of response of CZT/CdTe detectors compensating for and correcting problems related to trapping and low mobility of the charge carriers in these materials. In fact, these electrode configurations, with the implementation of appropriate logical reading of the signals, are intrinsically able to determine the position of interaction of the photon in the direction of the collected charge (depth sensing) and therefore are particularly suited to the realization of 3-D monolithic spectrometers without requiring a drastic increase of the electronics readout chains.

In the following sections, we will review a couple of configurations currently proposed and in development for the realization of 3-D spectrometers based on single large-volume crystals of CdTe/CZT. Even though there are other developments in this direction [41–44], the present choice is mainly dictated by application to hard x-rays and soft γ-rays, which requires good spatial resolution (at millimeter level or better) in all three dimensions coupled with fine and uniform spectroscopic response.

4.3.1 Pixel Spectrometers with Coplanar Guard Grid

By combining a pixelated anode array, already performing with good energy resolution because of the small pixel effect introduced in Section 2.2, and an interaction depth-sensing technique for electron-trapping corrections, it is possible to build CdZnTe γ-ray spectrometers with intrinsic 3-D position-sensing capability over quite large-volume (1–3 cm^3) bulk crystals. This configuration was proposed in 1998 by He et al. [45].

The first prototype was based on a $10 \times 10 \times 10$ cm^3 CZT crystal with an 11×11-pixel anode array and a single cathode electrode on the opposite surface [46]. The 2-D sensing of γ-ray interactions is simply provided by the pixel (x, y) anode, where electrons are collected on the anode surface. Instead of using an array of simple square pixel anodes, each square collecting anode is surrounded by a common noncollecting grid (Figure 4.6a and b). In the first configuration, the pixel pitch has dimensions of 0.7×0.7 mm^2, with a collecting anode of 0.2×0.2 mm^2 at the center surrounded by a common noncollecting grid with a width of 0.1 mm. Since the noncollecting grid is biased at lower potential relative to that of the collecting anodes, electrons are forced toward the collecting pixel anodes. Even more important, the dimension of the pixel collecting anode is small with respect to the anode–cathode distance and smaller than the geometrical pixel dimension, enhancing the small pixel effect and minimizing any induced signal from the holes' movement. To guarantee good electron collection, for this configuration the bias between anodes and the planar cathode is in the 1500–2000 V range, while the voltage difference between anodes and the noncollecting common grid is typically a few tenths of a volt (30–50 keV).

The γ-ray interaction depth between the cathode and the anode is obtained from the ratio between the signal readout by the cathode and the anode, respectively. With a simple coincidence logic between cathode and anode signals, this technique

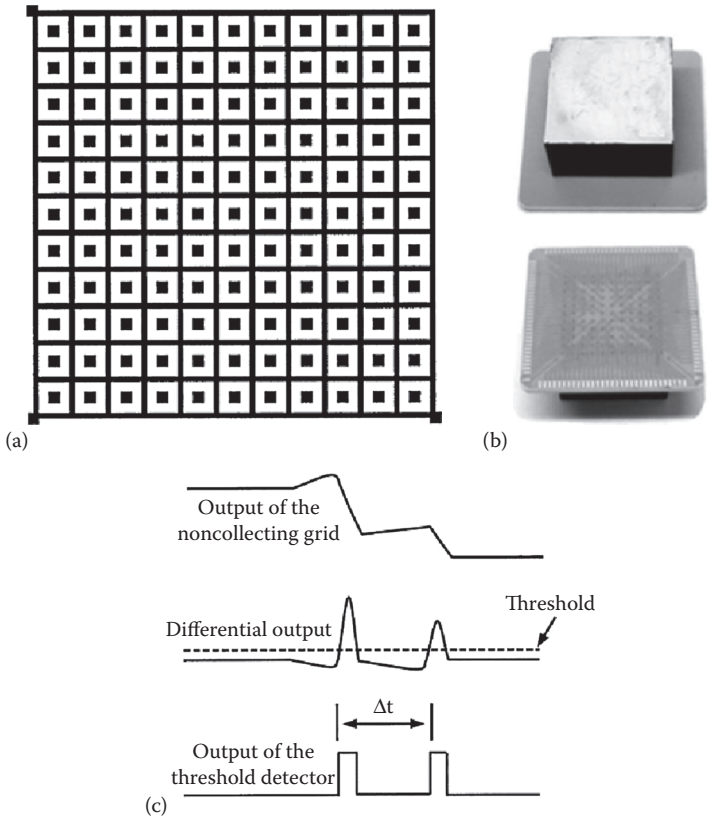

FIGURE 4.6 (a) Scheme of the anode side of the 10 × 10 × 10 mm^3 CZT prototype. (b) Photos of the detector (15 × 15 × 10 mm^3) with the ceramic substrate facing up (top) and with the cathode facing down (bottom), where, through the thin ceramic substrate, the anode bonding pad array is visible. (c) Scheme of the depth-sensing logic used for multiple-site event handling.

can provide the depth (z) of the photon interaction for single-site events, and only the centroid depth for multiple-site interactions (e.g., Compton-scattered events). In order to identify individual hit depths for multiple-site events, the signal from the noncollecting grid is also read out using a charge-sensitive preamplifier. When electrons generated by an energy deposition are detected toward the collecting pixel anode near the anode surface, a negative pulse is induced on the noncollecting grid, as shown in Figure 4.6c. This signal is differentiated, generating positive pulses corresponding to the slope inversion points of the noncollecting grid signal. Finally, a threshold circuit uses the differential output to provide a logic pulse when it is above a defined threshold [47]. These logic pulses provide start and stop signals to a time-to-amplitude converter (TAC) that measures the interval of drifting times of electrons.

By combining the centroid depth, pulse amplitudes from each pixel anode, and the depth interval between energy depositions derived from the measure of electron

drifting time, the depth of each individual energy deposition can be obtained. Although the differential circuit could identify multiple hits of the same incoming photon, the TAC limits the number of interactions to two. Therefore, the original system was able to provide interaction depths for only single and two-site (double) events. Events having more than two energy depositions can be identified by the number of anode-triggered pixels, but only the centroid interaction depth can be obtained. While the single-event low-energy threshold was low (~10 keV), the threshold for double events was relatively high, because their detection depended on the noncollecting grid signal threshold, which was, in the first measurements, in the order of 100 keV. The reconstructed interaction depth using this technique becomes worse with decreasing energy [48] and is ~0.25 mm for single events and ~0.4 mm for double ones at 662 keV.

In fact, since the first prototypes, several improvements have been realized by the same group on both the CZT sensor configuration and the readout and processing electronics, allowing the sensitive volume of each CZT device to be increased up to 6 cm^3 (i.e., $2\times2\times1.5$ cm^3) [49,50]. With these new sensors, very impressive spectroscopic performance can be achieved (Figure 4.7a) for all event types. These

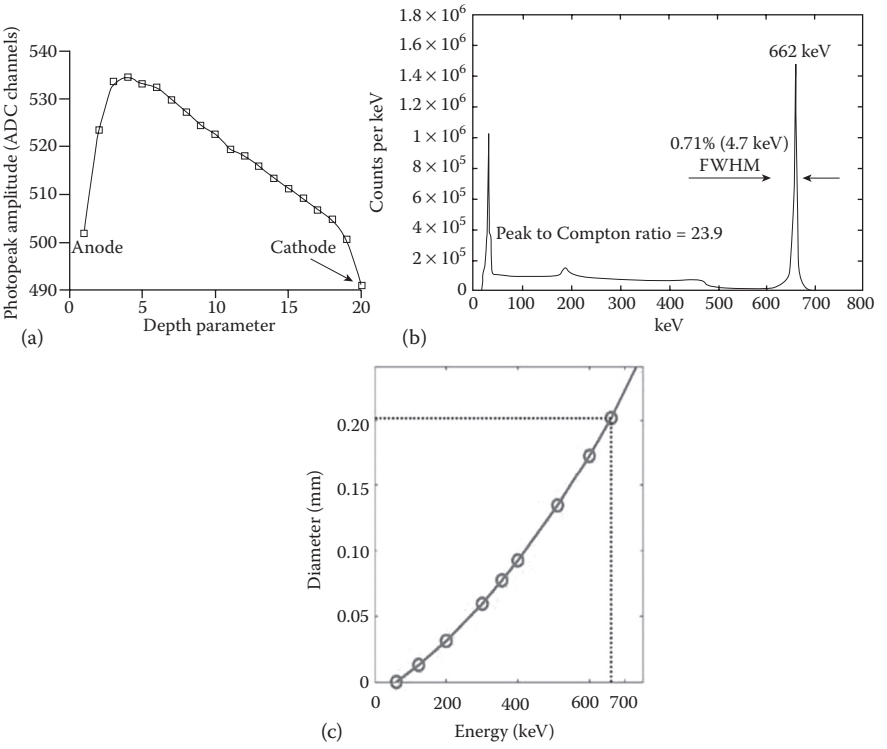

FIGURE 4.7 (a) The typical dependence of the centroids of ^{137}Cs photopeak from the interaction depth parameter (1 depth step = 0.5 mm) for one pixel. (b) ^{137}Cs spectrum measured by one pixel after compensation for interaction depth for all event multiplicity. (c) Diameter of the electron cloud generated by photon interaction vs. energy.

sensor units have been proposed as 3-D spectrometers for energy up to several megaelectronvolts. One of the main problems with operating in this energy region (>500 keV) is that the electron cloud, generated at each photon interaction point inside the sensitive volume, becomes larger than the pixels' lateral size (>1 mm) as the energy deposit increases. This effect, of course, tends to degrade the spatial resolution, because transient signals are collected by several anode pixels around the central one (charge sharing), which increases the uncertainty of depth reconstruction in the direction of charge collection.

Even if the geometrical spatial resolution in the anode plane of the larger CZT pixel sensor was at millimeter scale (1.8 mm pitch), with a custom-designed digital readout scheme, able to handle the signal coming from the eight pixels neighboring the triggered pixel, it has been demonstrated that a Δx of 0.23–0.33 mm can be achieved for a 662 keV single interaction [51].

Similar sensor configurations have been proposed, where the anode segmentation in a pixel array is replaced by a grid of orthogonal coplanar electrodes [52], as shown in Figure 4.8a, or by a parallel coplanar strip set [53] (Figure 4.8b), while maintaining in both cases a planar cathode on the opposite surface. The evident advantage of this detector scheme is the reduction of the required readout channels ($2N$) to achieve the same geometrical spatial resolution in the anode sensor plane (x, y) compared with an equivalent pixel array segmentation (N^2). In this case, the signal readout from the pixel lines gives one coordinate on the plane, while the orthogonal one is derived from analysis of the bipolar signals from noncollecting strips. As before, the third dimension (i.e., the interaction depth) can be inferred by the ratio between anode and cathode signals, but, due to the coplanar electrode configuration, the cathode signal can be replaced by the sum of all anode pixel line and strip signals. For a CZT detector of $10 \times 10 \times 10$ mm^3 with an orthogonal coplanar strip anode, the measurements have demonstrated that, despite a geometrical spatial resolution of

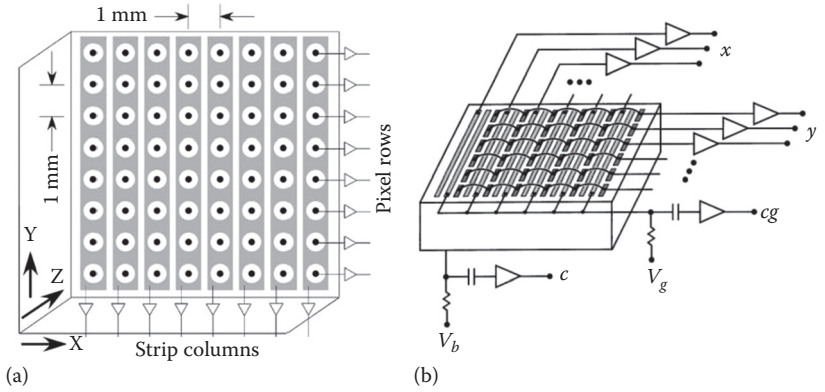

FIGURE 4.8 (a) Orthogonal coplanar-strip 3-D detector scheme: single-sided strip detector with collecting (row) and noncollecting (column) contacts on the anode surface. The cathode on the hidden side is planar. (b) Parallel coplanar-grid 3-D detector. The energy readout is accomplished by measuring the induced charge on a single set of interconnected anode strips, which are biased in order to collect the generated electrons.

1 mm in the (x, y) plane, the achievable 1σ values are between 0.2 and 0.4 mm for 122 and 60 keV, respectively, and ~0.4 mm in the interaction depth at 122 keV [54].

4.3.2 PTF Microstrip with Drift Configuration

Another way to build 3-D spectroscopic sensors relies on the use of CZT crystals in the PTF configuration. The drawback of the PTF irradiating geometry is that all the positions between the collecting electrodes are uniformly hit by impinging photons, leading to a stronger effect of the difference in charge-collection efficiency and thus in spectroscopic performance with respect to the standard irradiation configuration through the cathode (PPF). Therefore, worse spectroscopic performance can be expected in PTF with respect to the standard PPF irradiation configuration [55]. In order to recover from this spectroscopic degradation and to improve the CZT sensitive unit performance, an array of microstrips in a drift configuration can be used instead of a simple planar anode (Figure 4.9): the anode surface is made of a thin collecting anode strip surrounded by guard strips that are biased at decreasing voltages. This anode configuration [56] allows the detector to become almost a single-charge carrier device, avoiding the degradation of the spectroscopic response by charge loss due to hole trapping and providing a more uniform spectroscopic response (i.e., independent of the distance of the interaction from the collecting electrodes), as shown in Figure 4.10a [57]. The spectroscopic resolution of this type of sensor ranges from 6% at 60 keV down to 1.2% at 661 keV, without any correction for the interaction depth. In fact, similarly to the other configuration presented above, it will be possible to perform compensation of the collected charge signals using the photon interaction position within the metalized surface, which can be inferred by the ratio between the cathode and the anode strip signals [58].

The achievable spatial resolution in this direction is, of course, a function of energy, because the dimensions of the charge-generated cloud, up to 500 keV, have been measured [59] to be around 0.2 mm (Figure 4.10b). In order to obtain 3-D sensitivity for the photon interaction position, the cathode can also be segmented into strips in the direction orthogonal to the anode ones. Of course, with the described configuration, the spatial resolution along the anode surface is defined geometrically by the collecting anode and cathode strip pitch.

Both anode and cathode strips are read by standard spectroscopic electronics chains, and therefore the segmentation of both cathode and anode surface will set the number of readout channels. In fact, ongoing developments on this sensor configuration are demonstrating that, with a readout logic able to weight the signal between strips, the achievable spatial resolution also across the anode and the cathode strip sets can be better than the geometrical strip pitch. For a sensor unit similar to the one shown in Figure 4.11a, in which the cathode is segmented into 2 mm pitch strips, the final spatial resolution can be as low as 0.6 mm (up to 600 keV), weighting the cathode strip signals. In fact, also along the anodic strip set the effective resolution can be improved to a small fraction (1/5–1/10) of geometrical pitch between collecting strips by implementing an appropriate readout of the drift strip signal, similar to the one suggested by Luke et al. [60] for 3-D coplanar grid detectors [61].

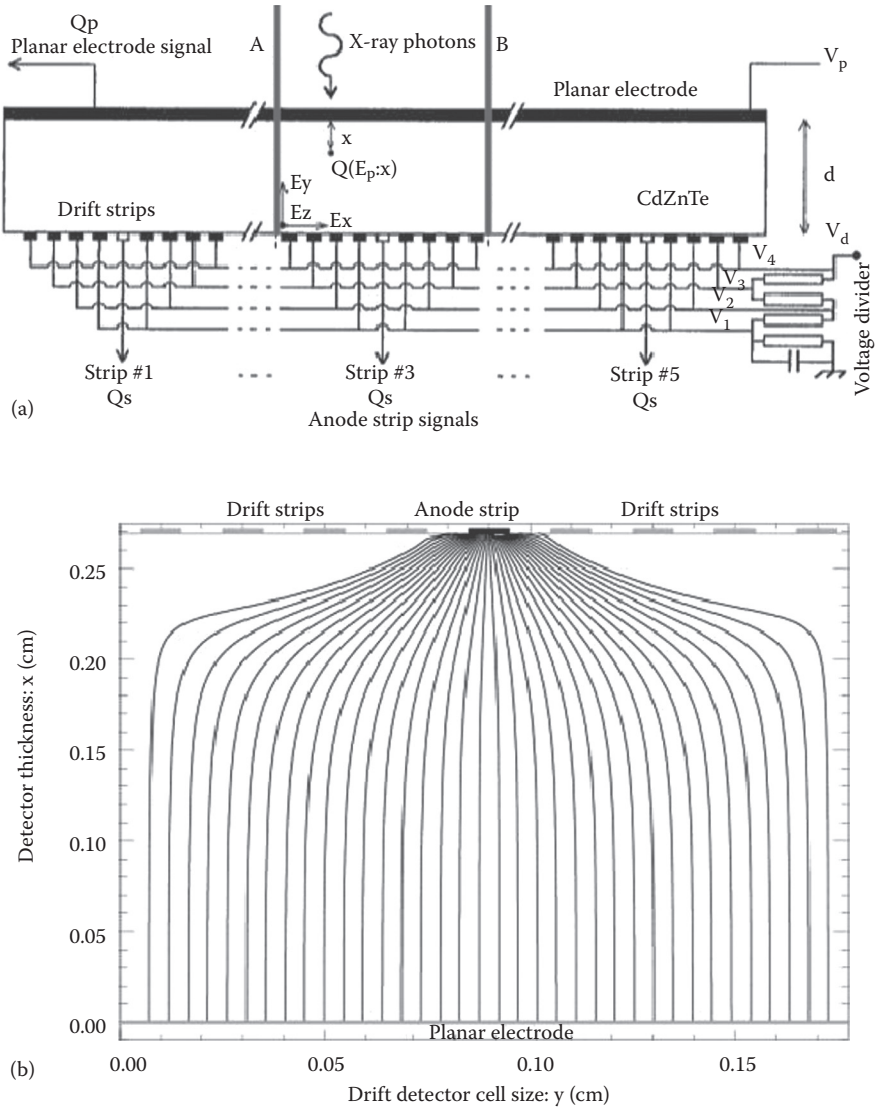

FIGURE 4.9 (a) Schematic configuration of a CZT drift-strip sensor. A drift-strip detector cell is shown between the two thick vertical lines marked "A" and "B." The drift-strip electrodes and the planar electrode are biased in such a way that the electrons move to the anode collecting strips (central white strips). (b) The shape of the charge-collecting field lines calculated for an anode cell on a CZT sensor with drift-strip electrode configuration (see Figure 4.8): the anode–cathode bias is set at 150 keV, and the difference between adjacent strips in pairs (ΔV) = –25 V.

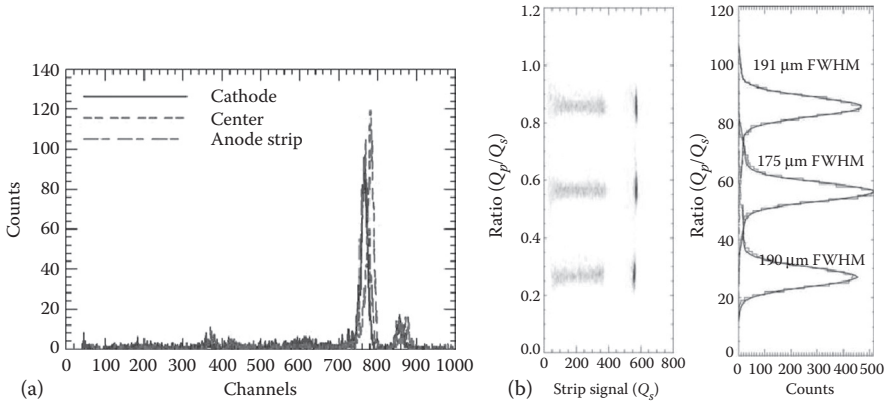

FIGURE 4.10 **(See color insert)** (a) Spectra of a collimated (0.6 mm spot) ^{57}Co source at three different positions between the collecting electrodes; the variation between the full energies peak and the corresponding energy resolution is within a few percent. (b) On the left, the biparametric distributions of the ratio between the planar electrode signal (Q_p) and the anode collecting-strip signal (Q_s) vs. Q_s for three positions of a 500 keV monochromatic x-ray beam; on the right, the corresponding measured depth resolution for these three different beam positions. The y-axis extension (ratio) is representative of the sensor interelectrode distance. The beam was collimated at 50 μm.

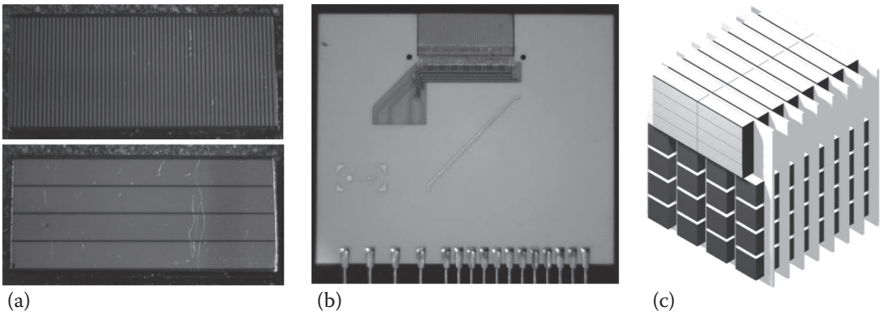

FIGURE 4.11 (a) Drift-strip CZT sensor ($18 \times 8 \times 2.5$ mm^3): (top) anode side with a set of 64 (0.15 mm wide) strips, (bottom) cathode side with four (2 mm wide) strips. (b) Linear module prototype seen from the anode side: this constitutes the basic element for building a large-volume 3-D sensor. (c) A suitable packaging scheme of eight linear modules, each supporting two CZT drift 3-D sensors of $20 \times 20 \times 5$ mm^3 to obtain a spectroscopic imager of 32 cm^3 sensitive volume.

Because of the use of the PTF configuration, the dimensions of the 3-D sensor unit can reach up to 20–30 mm in lateral size and up to 5 mm in charge-collecting distance, making it possible to limit the high bias voltage required to completely deplete the sensitive volume to values below 500 V. A particular implementation of these types of sensor is shown in Figure 4.11a, in which a CZT sensor of $18 \times 8 \times 2.4$ mm^3, with a fine-pitch μ-strip pattern on the CZT anode and a cathode segmented into four 2 mm wide orthogonal strips, is mounted on a 1 mm thick

alumina support. In this sensor prototype, there are four collecting anode strips, with an overall pitch of 2.4 mm, each one surrounded by four strips on each side, used as drift electrodes. While the bias between cathode and anode is typically 100 V mm^{-1}, the drift strips, to be effective in shaping the charge-collection field to minimize dead volume, are biased at decreasing relative voltage with respect to the cathode strips of $\Delta V = 20–30$ V. These values, of course, depend in particular on the thickness (distance between cathode and anode surfaces) of the sensor tile, and the best bias scheme must be carefully studied using charge transport models. Using such sensor units [62], a large-volume 3-D spectrometer can be built by packaging several units (as shown in Figure 4.11b and c), in which CZT 3-D sensors are bonded on a thin high-resistivity support layer (e.g., Al_2O_3), forming linear modules that provide the electrical interface for both readout electronics and bias circuits.

4.4 CONSIDERATIONS ON 3-D CZT/CdTe SPECTROMETER APPLICATIONS

The development of CZT/CdTe spectrometers with high 3-D spatial resolution and fine spectroscopy represents a real challenge to the realization of a new class of high-performance instruments able to fulfil current and future requirements in several application fields.

The possibility of also achieving a very good detection efficiency even at high energy (up to a few megaelectronvolts) [63], because of the sensitive volumes that can also be obtained by mosaics or stacks of 3-D sensor units, without significant loss of spectroscopic performance and response uniformity, together with their capability to operate at room temperature, makes them really appealing for application in radiation monitoring and identification [64] and homeland security, as well as in industrial noninvasive controls and, in the research field, for new hard x- and soft γ-ray astronomy instrumentation.

Furthermore, the fine spectroscopic resolution (a few percent at 60 keV and <1% above 600 keV) and the high 3-D spatial resolution (0.2–0.5 mm) that these devices can guarantee, coupled with high-performance readout electronics, allow operation not only in full energy mode but also as Compton-scattering or pair detectors if equipped with appropriate electronics providing a suitable coincidence logic to handle multihit events. These possibilities imply that these sensors are suitable to realize wide-field detectors for localization and detection of γ-ray sources (>100 keV) in both ground and space applications [65]. Evaluation using a single 3-D CZT sensor (Section 3.1) as a 4π Compton imager has demonstrated the possibility of obtaining an angular resolution ~15° at 662 keV. This is an excellent result in the small distance scale used to reconstruct Compton event kinematics, and can be achieved only because of the good 3-D and spectroscopic performance of the CZT proposed sensor units.

The possibility of operating 3-D spectrometers as Compton-scattering detectors gives the appealing opportunity to utilize these devices for measurements of hard x-ray and soft γ-ray polarimetry. Today, this type of measurement is recognized as being of fundamental importance in high-energy astrophysics, and is one of the most demanding requirements for instrumentation for the next space mission in

this energy range (10–1000 keV). The presence of linearly polarized photons in the incoming flux from a cosmic ray source determines a modulation in the azimuthal direction of Compton-scattered events [66]. A 3-D spectrometer able to properly handle scattered events is intrinsically able to measure these modulations, that is, to operate as a scattering polarimeter [67]. The quality (modulation factor) of a scattering polarimeter is strictly dependent on its spatial resolution and spectroscopic performance. Several experimental measurements [68,69] and simulation models have demonstrated that a detector allowing a good selection of events using both the spectroscopic and position information of each hit can achieve a very high modulation factor. In particular, the ability to select events within a thin layer of the sensitive volume, thanks to the intrinsic 3-D segmentation of the detector (i.e., close to 90° scattering direction), drastically improves the modulation factor and therefore the reliability of the polarimetric measurements.

REFERENCES

1. Pantazis, T., et al. (2010), The historical development of the thermoelectrically cooled x-ray detector and its impact on the portable and hand-held XRF industries, *X-Ray Spectrometry*, 39, 90.
2. Lechner, P., et al. (2004), Novel high-resolution silicon drift detectors, *X-Ray Spectrometry*, 33, 256.
3. Eberth, J. and Simpson, J. (2006), From Ge(Li) detectors to gamma-ray tracking arrays: 50 years of gamma spectroscopy with germanium detectors, *Progress in Particle and Nuclear Physics*, 60, 283.
4. Owens, A. and Peacock, A (2004), Compound semiconductor radiation detectors, *Nuclear Instruments and Methods in Physics Research A*, 531, 18.
5. Sellin, P.J. (2003), Recent advances in compound semiconductor radiation detectors, *Nuclear Instruments and Methods in Physics Research A*, 513, 332.
6. Lebrun, F., et al. (2003), ISGRI: The INTEGRAL soft gamma-ray imager, *Astronomy & Astrophysics*, 411, L141.
7. Lee, K., et al. (2010), Development of X-ray and gamma-ray CZT detectors for homeland security applications, *Proceedings of SPIE*, 7664, 766423–1.
8. Ogawa, K. and Muraishi, M. (2010), Feasibility study on an ultra-high-resolution SPECT with CdTe detectors, *IEEE Transactions on Nuclear Science*, 57, 17.
9. Limousin, O., et al. (2011), Caliste-256: A CdTe imaging spectrometer for space science with a 580 μm pixel pitch, *Nuclear Instruments and Methods in Physics Research A*, 647, 46.
10. Watanabe, S., et al. (2009), High energy resolution hard x-ray and gamma-ray imagers using CdTe diode devices, *IEEE Transactions on Nuclear Science*, 56, 777.
11. Berger, M.J., et al. (2010), XCOM: Photon cross sections database, National Institute of Standards and Technology, http://www.nist.gov/pml/data/xcom/index.cfm.
12. Cavalleri, G., et al. (1971), Extension of Ramo theorem as applied to induced charge in semiconductor detectors, *Nuclear Instruments and Methods in Physics Research*, 92, 137.
13. He, Z. (2001), Review of the Shockley–Ramo theorem and its application in semiconductor gamma ray detectors, *Nuclear Instruments and Methods in Physics Research A*, 463, 250.
14. Eskin, J.D., et al. (1999), Signals induced in semiconductor gamma-ray imaging detectors, *Journal of Applied Physics*, 85, 647.
15. Hecht, K. (1932), Zum Mechanismus des lichtelektrischen Primärstromes in isolierenden Kristallen, *Zeitschrift für Physik*, 77, 235.

16. Zanichelli, M., et al. (2013), Charge collection in semi-insulator radiation detectors in the presence of a linear decreasing electric field, *Journal of Physics D: Applied Physics*, 46, 365103.
17. Sato, G., et al. (2002), Characterization of CdTe/CdZnTe detectors, *IEEE Transactions on Nuclear Science*, 49, 1258.
18. Devanathan, R., et al. (2006), Signal variance in gamma-ray detectors: A review, *Nuclear Instruments and Methods in Physics Research A*, 565, 637.
19. Kozorezov, A.G., et al. (2005), Resolution degradation of semiconductor detectors due to carrier trapping, *Nuclear Instruments and Methods in Physics Research A*, 546, 207.
20. Casali, F., et al. (1992), Characterization of small CdTe detectors to be used for linear and matrix arrays, *IEEE Transactions on Nuclear Science*, 39, 598.
21. Caroli, E., et al. (2008), A three-dimensional CZT detector as a focal plane prototype for a Laue Lens telescope, *Proceedings of SPIE*, 7011, 70113G.
22. Jordanov, V.T., et al. (1996), Compact circuit for pulse rise-time discrimination, *Nuclear Instruments and Methods in Physics Research A*, 380, 353.
23. Richter, M. and Siffert, P. (1992), High resolution gamma ray spectroscopy with CdTe detector systems, *Nuclear Instruments and Methods in Physics Research A*, 322, 529.
24. Auricchio, N., et al. (2005), Twin shaping filter techniques to compensate the signals from CZT/CdTe detectors, *IEEE Transactions on Nuclear Science*, 52, 1982.
25. McGregor, D.S., et al. (1998), Single charge carrier type sensing with a parallel strip pseudo-Frisch-grid CdZnTe semiconductor radiation detector, *Applied Physics Letters*, 12, 192.
26. Bolotnikov, A.E., et al. (2006), Performance characteristics of Frisch-ring CdZnTe detectors, *IEEE Transactions on Nuclear Science*, 53, 607.
27. Barrett, H.H., et al. (1995), Charge transport in arrays of semiconductor gamma-rays detectors, *Physical Review Letters*, 75, 156.
28. Kuvvetli, I., and Budtz-Jørgensen, C. (2005), Pixelated CdZnTe drift detectors, *IEEE Transactions on Nuclear Science*, 52, 1975.
29. Luke, P.N. (1995), Unipolar charge sensing with coplanar electrodes: Application to semiconductor detectors, *IEEE Transactions on Nuclear Science*, 42, 207.
30. Shor, A., et al. (1999), Optimum spectroscopic performance from CZT γ- and x-ray detectors with pad and strip segmentation, *Nuclear Instruments and Methods in Physics Research A*, 428, 182.
31. Perillo, E., et al. (2004), Spectroscopic response of a CdTe microstrip detector when irradiated at various impinging angles, *Nuclear Instruments and Methods in Physics Research A*, 531, 125.
32. Lingren, C.L., et al. (1998), Cadmium-zinc telluride, multiple-electrode detectors achieve good energy resolution with high sensitivity at room-temperature, *IEEE Transactions on Nuclear Science*, 45, 433.
33. Kim, H., et al. (2004), Investigation of the energy resolution and charge collection efficiency of Cd(Zn)Te detectors with three electrodes, *IEEE Transactions on Nuclear Science*, 51, 1229.
34. Abbene, L., et al. (2007), Spectroscopic response of a CdZnTe multiple electrode detector, *Nuclear Instruments and Methods in Physics Research Section A*, 583, 324.
35. Frisch, O. (1944), British Atomic Energy Report, BR-49.
36. He, Z., et al. (1997), Position-sensitive single carrier CdZnTe detectors, *Nuclear Instruments and Methods in Physics Research A*, 388, 180.
37. Frontera, F., et al. (2013), Scientific prospects in soft gamma-ray astronomy enabled by the LAUE project, *Proceedings of SPIE*, 8861, 886106–1.
38. Della Monica Ferreira, D., et al. (2013), Hard x-ray/soft gamma-ray telescope designs for future astrophysics missions, *Proceedings of SPIE*, 886, 886116–1.

39. Watanabe, S., et al. (2002), CdTe stacked detectors for gamma-ray detection, *IEEE Transactions on Nuclear Science*, 49, 1292.
40. Judson, D.S., et al. (2011), Compton imaging with the PorGamRays spectrometer, *Nuclear Instruments and Methods in Physics Research A*, 652, 587.
41. Cui, Y., et al. (2008), Hand-held gamma-ray spectrometer based on high-efficiency Frisch-ring CdZnTe detectors, *IEEE Transactions on Nuclear Science*, 55, 2765.
42. Bale, D.S. and Szeles, C. (2006), Design of high performance CdZnTe quasi-hemispherical gamma-ray CAPture™ plus detectors, *Proceedings of SPIE*, 6319, 63190B.
43. Owens, A., et al. (2006), Hard x- and γ-ray measurements with a large volume coplanar grid CdZnTe detector, *Nuclear Instruments and Methods in Physics Research A*, 563, 242.
44. Dish, C., et al. (2010), Coincidence measurements with stacked (Cd,Zn)Te coplanar grid detectors, *2010 IEEE Nuclear Science Symposium Conference Record*, 3698.
45. He, Z., et al. (1999), 3-D position sensitive CdZnTe gamma-ray spectrometers, *Nuclear Instruments and Methods in Physics Research A*, 422, 173.
46. Stahle, C.M., et al. (1997), Fabrication of CdZnTe strip detectors for large area arrays, *Proceedings of SPIE*, 3115, 90.
47. Li, W., et al. (1999), A data acquisition and processing system for 3-D position sensitive CZT gamma-ray spectrometers, *IEEE Transactions on Nuclear Science*, 46, 1989.
48. Li, W., et al. (2000), A modeling method to calibrate the interaction depth in 3-D position sensitive CdZnTe gamma-ray spectrometers, *IEEE Transactions on Nuclear Science*, 47, 890.
49. Zhang, F., et al. (2004), Improved resolution for 3-D position sensitive CdZnTe spectrometers, *IEEE Transactions on Nuclear Science*, 51, 2427.
50. Zhang, F., et al. (2012), Characterization of the H3D ASIC readout system and 6.0 cm 3-D position sensitive CdZnTe detectors, *IEEE Transactions on Nuclear Science*, 59, 236.
51. Zhu, Y., et al. (2011), Sub-pixel position sensing for pixelated, 3-D position sensitive, wide band-gap, semiconductor, gamma-ray detectors, *IEEE Transactions on Nuclear Science*, 58, 1400.
52. Macri, J.R., et al. (2002), Study of 5 and 10 mm thick CZT strip detectors, *2002 IEEE Nuclear Science Symposium Conference Record*, 2316.
53. Luke, P.N. (2000), Coplanar-grid CdZnTe detector with three-dimensional position sensitivity, *Nuclear Instruments and Methods in Physics Research A*, 439, 611.
54. Macri, J.R., et al. (2003), Readout and performance of thick CZT strip detectors with orthogonal coplanar anodes, *2003 IEEE Nuclear Science Symposium Conference Record*, 468.
55. Auricchio, N., et al. (1999), Investigation of response behavior in CdTe detectors versus inter-electrode charge formation position, *IEEE Transactions on Nuclear Science*, 46, 853.
56. Gostilo, V., et al. (2002), The development of drift-strip detectors based on CdZnTe, *IEEE Transactions on Nuclear Science*, 49, 2530.
57. Caroli, E., et al. (2010), Development of a 3D CZT detector prototype for Laue Lens telescope, *Proceedings of SPIE*, 7742, 77420V.
58. Kuvvetli, I., et al. (2010), CZT drift strip detectors for high energy astrophysics, *Nuclear Instruments and Methods in Physics Research A*, 624, 486.
59. Kuvvetli, I., et al. (2010), Charge collection and depth sensing investigation on CZT drift strip detectors, *2010 IEEE Nuclear Science Symposium Conference Record*, 3880.
60. Luke, P.N., et al. (2000), Coplanar-grid CdZnTe detector with three-dimensional position sensitivity, *Nuclear Instruments and Methods in Physics Research A*, 439, 611.

61. Kuvvetly, I., et al. (2014), A 3D CZT high resolution detector for x-and gamma-ray astronomy, presented at High Energy, Optical, and Infrared Detectors for Astronomy VI, SPIE Astronomical Telescopes and Instrumentation Conference, 22–27 June 2014, Montréal, Quebec, Canada.
62. Auricchio, N., et al. (2012), Development status of a CZT spectrometer prototype with 3D spatial resolution for hard X ray astronomy, *Proceedings of SPIE*, 8453, 84530S.
63. Boucher, Y.A., et al. (2011), Measurements of gamma rays above 3 MeV using 3D position-sensitive $20 \times 20 \times 15$ mm^3 CdZnTe detectors, *2011 IEEE Nuclear Science Symposium Conference Record*, 4540.
64. Wahl, C.G. and He, Z. (2011), Gamma-ray point-source detection in unknown background using 3D-position-sensitive semiconductor detectors, *IEEE Transactions on Nuclear Science*, 58, 605.
65. Xu, D., et al. (2004), 4π Compton imaging with single 3D position sensitive CdZnTe detector, *Proceedings of SPIE*, 5540, 144.
66. Lei, F., et al. (1997), Compton polarimetry in gamma-ray astronomy, *Space Science Reviews*, 82, 309.
67. Xu, D., et al. (2005), Detection of gamma ray polarization using a 3-D position-sensitive CdZnTe detector, *IEEE Transactions on Nuclear Science*, 52, 1160.
68. Curado da Silva, R.M., et al. (2011), Polarimetry study with a CdZnTe focal plane detector, *IEEE Transactions on Nuclear Science*, 58, 2118.
69. Antier, S., et al. (2014), Hard X-ray polarimetry with Caliste, a high performance CdTe based imaging spectrometer, *Experimental Astronomy*, (in press).

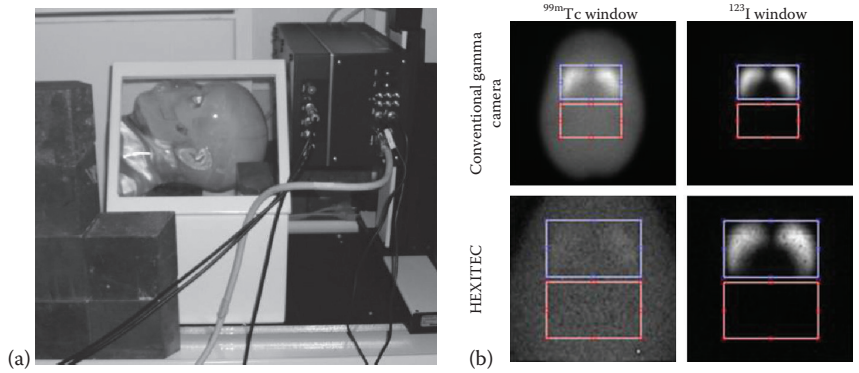

FIGURE 3.19 (a) Dual isotope SPECT imaging of an anthropomorphic brain phantom using the HEXITEC detector. The majority of the phantom is filled with ^{99m}Tc, while the striatal compartments are filled with ^{123}I. (b) A comparison of the imaging performance of a traditional GE Infinia γ camera and the HEXITEC detector system. Images are shown for energy windows around the principal emissions of the ^{99m}Tc and ^{123}I radioisotopes. The use of the HEXITEC detector greatly reduces the cross talk between the two images.

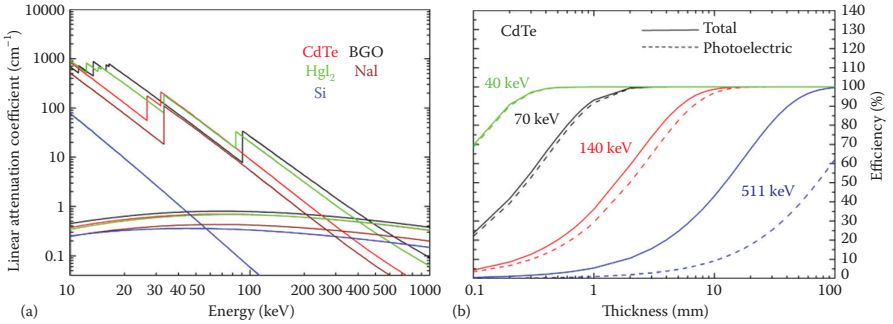

FIGURE 4.1 (a) Linear attenuation coefficients for photoelectric absorption and Compton scattering of CdTe, Si, HgI_2, NaI, and BGO. (b) Efficiency of CdTe detectors as a function of detector thickness at various photon energies.

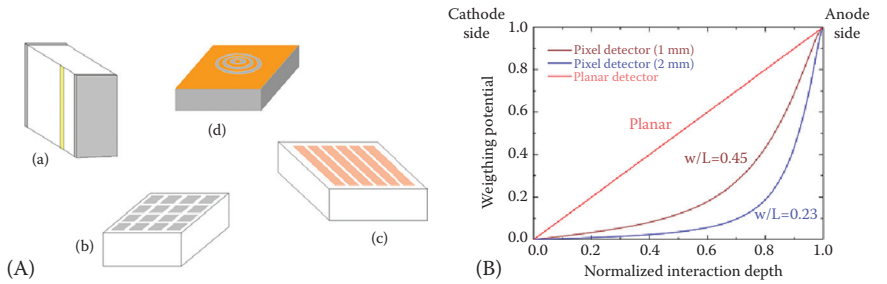

FIGURE 4.5 (A) Single-charge collection electrode configurations widely used in CdTe and CdZnTe detectors: (a) parallel-strip Frisch grid, (b) pixel, (c) strip, and (d) multiple electrodes. (B) Weighting potential of a pixel detector, compared with a planar detector. It is possible to improve the unipolar properties of pixel detectors by reducing the *w/L* ratio (i.e., pixel size to detector thickness), according to the theory of small pixel effect.

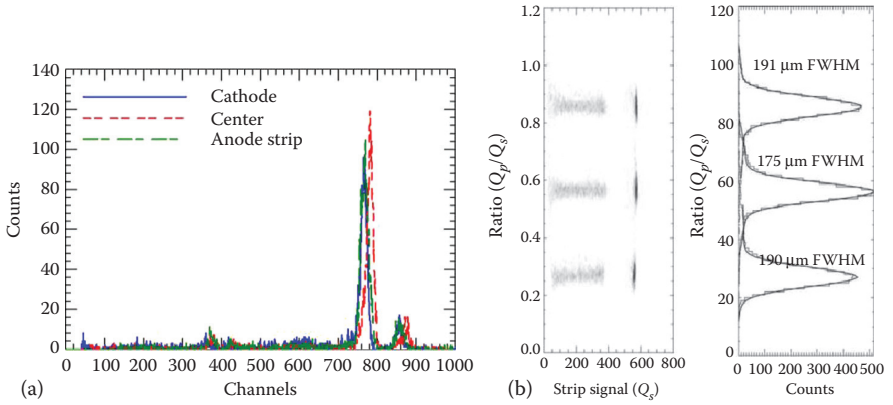

FIGURE 4.10 (a) Spectra of a collimated (0.6 mm spot) ^{57}Co source at three different positions between the collecting electrodes; the variation between the full energies peak and the corresponding energy resolution is within a few percent. (b) On the left, the biparametric distributions of the ratio between the planar electrode signal (Q_p) and the anode collecting-strip signal (Q_s) vs. Q_s for three positions of a 500 keV monochromatic x-ray beam; on the right, the corresponding measured depth resolution for these three different beam positions. The y-axis extension (ratio) is representative of the sensor interelectrode distance. The beam was collimated at 50 µm.

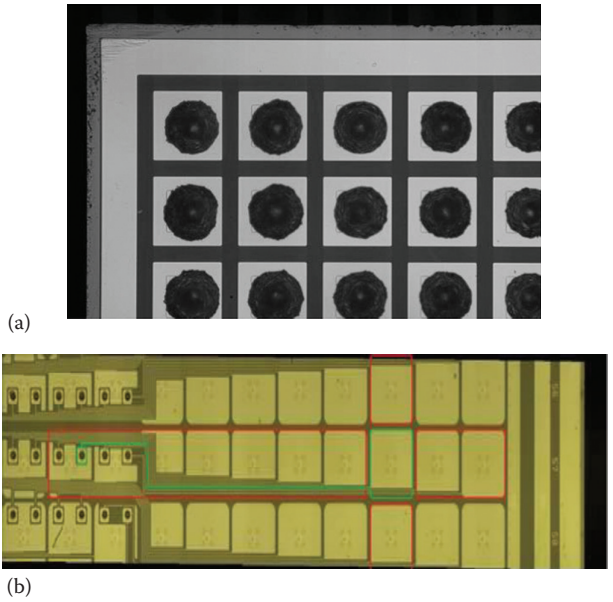

FIGURE 6.3 (a) Hexitec CdTe 250 µm pitch pad geometry with silver glue dots. (b) XFEL LPD redistributed bonding pads 250 × 400 µm^2 pitch (left) to the 500 µm pitch pixels on a two-layer interconnect silicon detector.